Hillman, Timothy; Zhang, Nan; Jin, Zhuo

Article

Real-option valuation in a finite-time, incomplete market with jump diffusion and investor-utility inflation

Risks

Provided in Cooperation with:
MDPI – Multidisciplinary Digital Publishing Institute, Basel

Suggested Citation: Hillman, Timothy; Zhang, Nan; Jin, Zhuo (2018) : Real-option valuation in a finite-time, incomplete market with jump diffusion and investor-utility inflation, Risks, ISSN 2227-9091, MDPI, Basel, Vol. 6, Iss. 2, pp. 1-20, https://doi.org/10.3390/risks6020051

risks

MDPI

Article

Real-Option Valuation in a Finite-Time, Incomplete Market with Jump Diffusion and Investor-Utility Inflation

Timothy Hillman [1], Nan Zhang [2,1,*] and Zhuo Jin [1]

[1] Centre for Actuarial Studies, Department of Economics, The University of Melbourne, VIC 3010, Australia; thillman@student.unimelb.edu.au (T.H.); zjin@unimelb.edu.au (Z.J.)

[2] School of Statistics, East China Normal University, 500 Dongchuan Road, Shanghai 200241, China

* Correspondence: nzhang@sfs.ecnu.edu.cn; Tel.: +86-21-5434-5058

Received: 18 March 2018; Accepted: 24 April 2018; Published: 4 May 2018

Abstract: We extend an existing numerical model (Grasselli (2011)) for valuing a real option to invest in a capital project in an incomplete market with a finite time horizon. In doing so, we include two separate effects: the possibility that the project value is partly describable according to a jump-diffusion process, and incorporation of a time-dependent investor utility function, taking into account the effect of inflation. We adopt a discrete approximation to the jump process, whose parameters are restricted in order to preserve the drift and the volatility of the project-value process that it modifies. By controlling for these low-order effects, the higher-order effects may be considered in isolation. Our simulated results demonstrate that the inclusion of the jump process tends to decrease the value of the option, and expand the circumstances under which it should be exercised. Our results also demonstrate that an appropriate selection of the time-dependent investor utility function yields more reasonable investor-behaviour predictions regarding the decision to exercise the option, than would occur otherwise.

Keywords: real option; incomplete market; jump diffusion; time-dependent risk preferences

1. Introduction

We consider the problem of valuing a real option, a derivative providing the right to undertake in a capital investment project, or in general, to invest in a given real asset within a specified time period. More details about real options in investment are provided in Dixit and Pindyck (1994). We begin with the formalism developed in Grasselli (2011); the results in the current manuscript are based on the numerical model presented in this reference. The distinguishing characteristics of the Grasselli approach were that it enabled the real option to be valued in an *incomplete market*, within a *finite time horizon*.

In an incomplete market, the time-varying value of the real project under consideration is *not* perfectly correlated to a traded financial asset (or a stock market index), so that the option value cannot be fully hedged. Thus, its value depends to a degree on the investor's (or the implied market) risk preferences. The finite time horizon, (or investment period) meant that the option value and the minimum project value at which its exercised both depend on the time until expiry. In Grasselli (2011), an exponential utility function is used to model the investor's risk preferences, following work by Hugonnier and Morellec (2007) and Henderson (2007) (which utilised an infinite time horizon). A binomial tree model in the manner of Cox, Ross and Rubenstein Cox et al. (1979) is used for computational calculations.

For the purposes of the current manuscript, we incorporate two extensions into the numerical model. In Grasselli's work, the risk-aversion coefficient γ, the parameter of the investor's utility

function, is constant over the lifetime of the project, and applied to the discounted monetary units at each backward induction step on the binomial tree. It implicitly assumes that the "inflation rate" applied to the nominal monetary amounts to which the investor assigns a fixed utility level over time, is equal to the risk-free interest rate. This may not be the case.

Extending this idea further, some recent literature has stated that a constant risk-aversion coefficient is unrealistic and may introduce substantial decision biases to the optimal strategies. Thaler (1981) shows that there exists some empirical evidence about dynamic inconsistencies in the discount factors. Loewenstein and Prelec (1992) studies the time-inconsistency when making decisions and provides an economic explanation. Yong (2012) derives optimal strategies for time-inconsistent optimal control problems based on the method of Hamilton-Jacob-Bellmen equations. Zhao et al. (2014) analyzed the optimal dividend payment strategies under the assumption of time-inconsistent preferences. Some related work about time-inconsistent preferences includes Ainslie (1992); Grenadier and Wang (2007) and Chen et al. (2014).

To reflect the time-inconsistency in the decision making process, we suggest that the project inflation rate, α, may better characterise the investor's time-dependent risk preferences (than the risk-free rate). Regardless, our first extension is introduce a new parameter, i, which characterises the investor's implicit inflation rate. Then, we replace the coefficient γ with a time-varying substitute, γ_t, which decays exponentially (with time t) at a rate determined by the difference between i and the risk-free rate r.

The second extension is to introduce a jump-diffusion component into the model. It is well known that the Black-Scholes model fails to capture the volatility smiles and fat tails that have been observed in financial markets since the late 1980s. Since then, much work has sought to overcome its drawbacks. Jump-diffusion models are among one of the most popular alternative models because of their advantage in describing the short-run behaviour of security prices. Kou and Wang (2004) studied exotic options under a double-exponential jump-diffusion model. A mixed-exponential jump-diffusion model is proposed in derivative pricing in Cai and Kou (2011). Work related to jump-diffusion models includes Merton (1976), Pham (1997), Song et al. (2006) and Bonis et al. (2009). For our purpose, the justification is that the estimated value of the project is likely to not vary in a continuous manner according to geometric Brownian motion, but instead, to be subject to a number of intermittent adjustments (jumps), reflecting new information about project profitability or viability. The jump-diffusion process (or jump process) may be treated as uncorrelated with the performance of the traded asset (or index). Therefore, we treat it as a component of the non-hedgeable source of fluctuations in the project-value process.

In this work, we utilise a double-exponential distribution to represent the logarithm of the jump magnitude, with the number of jumps occurring up to a given time following a Poisson process. Compared with the double-exponential distribution adopted in Kou and Wang (2004), the parameters of the jump process were subject to an important restriction: incorporation of this process into the project-value process should not alter the drift or volatility of the latter. This is for two reasons. First and most importantly, it permits us to control for these dominant low-order effects (drift, volatility), which can be modified through the other parameters of the project-value process. (We can isolate the higher-order effects that are unique to the jump-diffusion model.) The second reason is that it permits us to represent the process with fewer free parameters. To apply the jump process on the binomial tree, we represented the double-exponential distribution in discrete form, using an approach by Luceño (1999) in order to match both the low-order moments and the cumulative distribution function of the continuous random variable to reasonable accuracy.

In the subsequent sections of this manuscript, we describe our modifications to the Grasselli algorithm, and present and discuss some numerical results highlighting their effects. Because of its importance in investor decision making, we follow Grasselli and his predecessors in emphasising the option's exercise threshold value, the minimum project value (at any time) for which the option should be exercised immediately. We also afford significance to the *time value* of the option, the difference

between its current value and the maximum of its immediate exercise value or zero. We present colour maps of this quantity vs. both time and project value. We compare different cases according to the values they assign to the option when the project value is "at the money".

The structure of the remainder of this manuscript is as follows. In Section 2, we provide a general mathematical model for the random processes describing the project and stock price movements (Section 2.1), and present our representation of the investor's time-dependent utility function (Section 2.2). The specific form of the jump process, based on a double-exponential jump distribution, is given in Section 3. In its three constituent sections, we present, respectively: the jump distribution itself, including parameter limitations; the backwards induction step on our multinomial tree; and the method for discretising the jump distribution. Section 4 follows by providing more detailed specifics of the numerical algorithm we used in our calculation, including the justification for the selection of numerical parameters. We provide some results of the simulation in Section 5, highlighting the different issues we raise in the manuscript. Section 5.1 demonstrates the significance of the time dependence of the investor utility function, and Section 5.2 the effect of varying inflation. In both preceding cases, jump diffusion is not incorporated into the model, in order to target these alternative effects. Instead, it is investigated in Section 5.3, which shows the effects of varying all of its major parameters. Our conclusions are summarised in Section 6.

2. Model Description

2.1. Fundamentals of the Model

We consider a market in which there are two liquidly traded assets, a stock (index) with value $\tilde{S}(t)$ at time t, and a riskless bond, with value $\tilde{B}(t)$, for which $\tilde{B}(0) = 1$.

There also exists a project, whose value at time t is represented by $\tilde{V}(t)$, which is not traded. However, a *real option* exists, which, at the option-holder's choice, may be exercised at any time t satisfying $0 \leq t \leq T$, where the upper limit T is the finite *stopping time* of the project. If exercised at time t, the option provides an immediate payoff of $\tilde{V}(t) - \tilde{I}(t)$, where $\tilde{I}(t)$ is the time-dependent strike price, a deterministic function of time defined in the option contract.

We assume that $\tilde{S}(t)$ obeys geometric Brownian motion, and that the random process for $\tilde{V}(t)$ is Markovian and time-homogeneous. As in Grasselli (2011), it is partially correlated with $\tilde{S}(t)$. In our case, however, it is not restricted to following geometric Brownian motion. The quantities $\tilde{B}(t)$ and $\tilde{I}(t)$ are assumed to be increasing exponentially with time, with continuous compounding rates r and α, respectively. The rate r is the risk-free interest rate, and α is an inflation rate that is specified in the terms of the contract. Quite possibly $\alpha = 0$.

The effect of the non-zero riskless interest rate can be removed by expressing $\tilde{S}$, $\tilde{V}$, $\tilde{B}$, and $\tilde{I}$, in discounted coordinates, to yield S, V, B, and I, respectively. That is, we divide the former quantities by the common *numeraire* $\tilde{B}$. Letting ν_n be the arrival time of the n-th jump, then $N(t) = \max\{n \in \mathbb{N} : \nu_n \leq t\}$ is the number of jumps up to time t, a Poisson counting process. Let $X(t)$ be a jump process representing the sum of jumps, which are denoted by $\mathcal{J}(\cdot)$, with arrival rate λ and jump size density distribution $f(\cdot)$. That is $X(t) = \sum_{k=1}^{N(t)} \mathcal{J}(k)$.

The discounted quantities obey the following rules (Grasselli 2011, Equation (1)):

$$dS(t) = (\mu_1 - r)S(t)dt + \sigma_1 S(t)dW_t^1, \tag{1}$$

$$d(\log V(t)) = \left(\mu_2 - r - \frac{\sigma_2^2}{2} + \left[\frac{\sigma_2^2\rho_X^2}{2} - \lambda E(e^{\rho_X\sigma_2\mathcal{J}} - 1)\right]\right)dt + \sigma_2\left(\rho dW_t^1 + \sqrt{1-\rho^2-\rho_X^2}dW_t^2 + \rho_X dX(t)\right), \tag{2}$$

$$B(t) = 1, \tag{3}$$

$$dI(t) = (\alpha - r)I(t)dt. \tag{4}$$

We also assume that $I(0) = 1$ (by appropriately selecting both monetary units and the bond size at time $t = 0$), and require that the parameters ρ, ρ_X satisfy the condition $\rho^2 + \rho_X^2 \leq 1$.

The random processes $X(t)$, W_t^1 and W_t^2 (the last-mentioned two being Brownian motions) are assumed to be independent, so that, in particular, the random components of $S(t)$ and $V(t)$ are only dependent on each other through W_t^1, with the correlation term ρ indicating the magnitude of this dependence. The terms μ_1, μ_2 represent the drifts of $\tilde{S}(t)$, $\tilde{V}(t)$, respectively, and positive σ_1, σ_2 represent their volatilities.

In Grasselli (2011), $V(t)$ evolved in time according to geometric Brownian motion, that is, ρ_X was equal to zero. The more general form of $X(t)$ permits us to incorporate other models of project-value movements, such as jump diffusion, into the formulation. Equation (2) is expressed in terms of $\log V(t)$, rather than $V(t)$, to permit the choice of distribution for $X(t)$ to be incorporated into the multinomial tree we develop in Section 3.2 without modification, since the tree utilises a logarithmic scale for $V(t)$. The mean and variance of $X(t)$ are selected to be equal to those of W_t^1 and W_t^2. That is, $E[X(t)] = 0$, $\mathrm{Var}[X(t)] = t$. This is to ensure that the parameter σ_2 is meaningful as a measure of volatility. The correction terms $\sigma_2^2\rho_X^2/2 - \lambda E(e^{\rho_X\sigma_2\mathcal{J}} - 1)$ in Equation (2) are necessary to ensure that μ_2 represents the drift of $\tilde{V}(t)$, regardless of the value of ρ_X.

The market is incomplete, since it is not possible to replicate the variations of the value of the project by merely dynamically trading the stock and the bond. Thus, there will not be a unique arbitrage-free price for the real option. In order to calculate a price, the option holder's risk preferences must be taken into account. We represent the risk preferences by a utility function $U_t(\cdot)$; the potential investor will seek to maximise their expected utility at any given time. The subscript t represents the possible explicit time-dependence of the utility function, an idea we develop in Section 2.2.

Based on this formulation, the value of the option at any time t can be expressed $D(t; V(t), W)$. The parameter W represents the investor's total wealth at time t, which may influence their risk preferences, given the utility function. Our aim is to calculate the quantity D using backwards induction on the multinomial tree.

The fact that $dS(t)/S(t)$ is independent of $S(t)$, guarantees that, at a given time t, the option price $D(t)$ does not depend on the current value of $S(t)$. This is because for any dynamic trading strategy, the quantity $dS(t)/S(t)$ will be equal to the incremental proportional change in the total investor wealth invested in the stock, regardless of the price of an individual unit of stock. Thus, as in Grasselli (2011), a one-dimensional tree is sufficient to calculate D. Also, we may write $D \equiv D(t; V(t))$, suppressing the notation indicating the explicit dependence on W.

2.2. Time-Dependence of the Exponential Utility Function

The calculation of the option value is considerably simplified if we adopt an exponential utility function $U_t(x) = -\exp(-\gamma_t x)$. This is due to the fact that an investor whose utility can be described in this way exhibits constant absolute risk aversion, with risk aversion parameter γ_t. As such, the initial value of the investor's total wealth, W_0, is irrelevant in determining the option price D.

We have incorporated time-dependence into the utility function for two reasons. Firstly, the monetary values x we shall use in our calculation will be represented in terms of their present values at time 0, according to discount rate r. However, at any time t, when an investor is making a decision about whether to exercise the option, the quantities of money considered will be in terms of their undiscounted values *at time t*. Therefore, the factor γ_t should be appropriately scaled in order to reverse the discounting effect.

The second reason why time-dependence should be incorporated into the utility function is that the investor's risk preferences may change over time. We denote by i the inflation rate that applies to monetary values over time to which the investor assigns a fixed utility level. Its effect on γ_t is to impart an exponential decay factor at rate i. This corrects the product $\gamma_t x$ for the fact that x is expressed in nominal, not real monetary units.

Thus, in order that the utility function captures both of these time-dependent effects, correction for discounting, and the investor's implicit inflation considerations, then:

$$\gamma_t = \gamma_0 \exp\left[-(i-r)t\right], \tag{5}$$

where γ_0 is the risk-aversion parameter at time 0.

Note that in Grasselli (2011), a constant value $\gamma_t = \gamma$ is used at all times. In terms of Equation (5), this would imply that $r = i$, that is, an investor's relative risk treatment of different monetary amounts would vary in accordance with the risk-free rate r. In practice, it may be more likely that $i = \alpha$ better describes the investor's behaviour: their risk-attitude towards the real value of a project remains stable over time. We shall compare the two cases in our subsequent calculations.

3. Jump-Diffusion Model

3.1. Distribution of the Jump Process

We specify a form for the jump process $\{X(t)\}|_{t\in[0,T]}$. The jumps occur according to a Poisson process with rate λ, and with the following properties. In a short interval ΔT,

$$\Delta X \equiv X(t+\Delta T) - X(t) = \begin{cases} 0, & \text{with probability } 1-\lambda\Delta T + o(\Delta T), \\ \mathcal{J}, & \text{with probability } \lambda\Delta T + o(\Delta T), \\ \text{Multiple jumps}, & \text{with probability } o(\Delta T). \end{cases} \tag{6}$$

We assume that $\mathcal{J}$ is distributed according to a double-exponential distribution demonstrated in Kou and Wang (2004), with parameters $0 \le p_X \le 1, \eta_1 > 0, \eta_2 > 0$, so that its probability density function:

$$f(x) = \begin{cases} (1-p_X)\eta_2 \exp(\eta_2 x), & \text{if } x < 0, \\ p_X \eta_1 \exp(-\eta_1 x), & \text{if } x \ge 0. \end{cases} \tag{7}$$

Thus, the random process $\{X(t)\}$ is characterised by the four parameters p_X, η_1, η_2 and λ. However, if these parameters are allowed to vary freely, their selection may introduce additional volatility into the project value, a parameter that we wish to control for as noted in the Introduction. Instead, volatility (and drift) can be modified through the parameters σ_2, μ_2 in Equation (2). Thus, we restrict the parameters of $X(t)$, matching the first and second moments of the random variables $X(t)$ and W_t^2, for all t. As a result, the volatility of $V(t)$ will not depend on ρ_X. The drift of $V(t)$ was already controlled by the correction terms (in Equation (2)), described in Section 2.1. However, matching the first moments of the random variables provides first-order correction. Given these restrictions, we may characterise $\{X(t)\}$ in terms of two free parameters instead of four. They are λ and $\chi \equiv \eta_2/\eta_1$. The other original parameters can be expressed in terms of λ and χ as follows:

$$p_X = \frac{1}{1+\chi}; \qquad \eta_1 = \sqrt{\frac{2\lambda}{\chi}}; \qquad \eta_2 = \sqrt{2\lambda\chi}. \tag{8}$$

Finally, the parameter χ is related to the skewness Sk_X, the scaled third moment of ΔX, according to the equation:

$$\mathrm{Sk}_X = \frac{3}{\sqrt{2}}\left(\sqrt{\chi} - \sqrt{1/\chi}\right). \tag{9}$$

3.2. Setup of the Multinomial Tree

The multinomial tree is set up in a similar manner to that of Grasselli (2011). We define the time step to be ΔT. Then consider a single step, from time t to time $t+\Delta T$. We wish to calculate the value

of the option $D(t)$, given a particular current value for the project, $V(t)$, and the values of the option for all project values at time $t + \Delta T$.

Following (Grasselli 2011, Equation (29)), we let the ordered pair (S_t, V_t) evolve over a time step as follows:

$$(S_{t+\Delta T}, V_{t+\Delta T}) = \begin{cases} (uS_t, hV_t), & \text{with probability } p_1(1-\lambda\Delta T), \\ (uS_t, \ell V_t), & \text{with probability } p_2(1-\lambda\Delta T), \\ (dS_t, hV_t), & \text{with probability } p_3(1-\lambda\Delta T), \\ (dS_t, \ell V_t), & \text{with probability } p_4(1-\lambda\Delta T), \\ (uS_t, V_t \exp(\Delta X_d)), & \text{with probability } (p_1+p_2)\lambda\Delta T, \\ (dS_t, V_t \exp(\Delta X_d)), & \text{with probability } (p_3+p_4)\lambda\Delta T, \end{cases} \tag{10}$$

where the random variable ΔX_d is a discrete approximation of the random variable $\sigma_2\rho_X\Delta X$. This will approximate the evolution of the random process to order ΔT.

The values u, d, h, ℓ apply the binary "up-down", "high-low" factors to S and V, and the probabilities p_1, p_2, p_3, p_4 associated with the four options (two binary choices) are similar to their respective values derived in (Grasselli 2011, Equations (46)–(51)). However, they must be corrected to take into account the fact that the volatility σ_2 is partially allocated to the jump-diffusion term in Equation (2).

Based on the actual stock price $S(t)$ and project value $V(t)$, up to the order ΔT, we work with the increments relating up to down and high to low,

$$\begin{aligned} u &= 1/d = \exp\left(\sigma_1\sqrt{\Delta T}\right), \\ h &= 1/\ell = \exp\left(\sigma_2\sqrt{\Delta T\left(1-\rho_X^2\right)}\right), \end{aligned}$$

where u and h are multipliers on the stock price for an up move and a down move, respectively.

Following the procedure in Grasselli (2011), we work with the logarithms of the geometric Brownian motions of $S(t)$ and $V(t)$, i.e., $Y_t^1 = \log S(t)$ and $Y_t^2 = \log V(t)$ respectively, to simplify the calculation. Under the condition that there is no jump in the project value during the time step, we match the mean and covariance matrix for the discrete-time process on the binomial tree with increments $(\Delta y_1, \Delta y_2)$ with those of the continuous-time process (Y_t^1, Y_t^2) up the order ΔT. Denoting $\nu_i = \mu_i - r - \sigma_i^2/2, i = 1, 2$, we have (Grasselli 2011, Equations (38)–(42)):

$$\begin{aligned} E[\Delta Y_t^1 \mid \Delta X = 0] &= (p_1 + p_2 - p_3 - p_4)\Delta y_1 = \nu_1\Delta T, \\ E[\Delta Y_t^2 \mid \Delta X = 0] &= (p_1 - p_2 + p_3 - p_4)\Delta y_2 = \left[\nu_2 + \frac{\sigma_2^2\rho_X^2}{2} - \lambda E(e^{\rho_X\sigma_2\mathcal{J}} - 1)\right]\Delta T, \\ E[(\Delta Y_t^1)^2 \mid \Delta X = 0] &= (p_1 + p_2 + p_3 + p_4)(\Delta y_1)^2 = \sigma_1^2\Delta T, \\ E[(\Delta Y_t^2)^2 \mid \Delta X = 0] &= (p_1 + p_2 + p_3 + p_4)(\Delta y_2)^2 = \sigma_2^2(1-\rho_X^2)\Delta T, \\ E[\Delta Y_t^1\Delta Y_t^2 \mid \Delta X = 0] &= (p_1 - p_2 - p_3 + p_4)\Delta y_1\Delta y_2 = \rho\sigma_1\sigma_2\Delta T, \end{aligned}$$

where:

$$\begin{aligned} \Delta y_1 &= \sigma_1\sqrt{\Delta T}, \\ \Delta y_2 &= \sigma_2\sqrt{\Delta T(1-\rho_X^2)}. \end{aligned}$$

Solving this linear system, we obtain the unique solution:

$$\begin{aligned}
p_1 &= \frac{1}{4}\left[1+\frac{\rho}{\sqrt{1-\rho_X^2}}+\sqrt{\Delta T}\left(\frac{\nu_1}{\sigma_1}+\frac{\nu_2+\sigma_2^2\rho_X^2/2-\lambda E[e^{\rho_X\sigma_2\mathcal{J}}-1]}{\sigma_2\sqrt{1-\rho_X^2}}\right)\right],\\
p_2 &= \frac{1}{4}\left[1-\frac{\rho}{\sqrt{1-\rho_X^2}}+\sqrt{\Delta T}\left(\frac{\nu_1}{\sigma_1}-\frac{\nu_2+\sigma_2^2\rho_X^2/2-\lambda E[e^{\rho_X\sigma_2\mathcal{J}}-1]}{\sigma_2\sqrt{1-\rho_X^2}}\right)\right],\\
p_3 &= \frac{1}{4}\left[1-\frac{\rho}{\sqrt{1-\rho_X^2}}+\sqrt{\Delta T}\left(-\frac{\nu_1}{\sigma_1}+\frac{\nu_2+\sigma_2^2\rho_X^2/2-\lambda E[e^{\rho_X\sigma_2\mathcal{J}}-1]}{\sigma_2\sqrt{1-\rho_X^2}}\right)\right],\\
p_4 &= \frac{1}{4}\left[1+\frac{\rho}{\sqrt{1-\rho_X^2}}+\sqrt{\Delta T}\left(-\frac{\nu_1}{\sigma_1}-\frac{\nu_2+\sigma_2^2\rho_X^2/2-\lambda E[e^{\rho_X\sigma_2\mathcal{J}}-1]}{\sigma_2\sqrt{1-\rho_X^2}}\right)\right],
\end{aligned}$$

where

$$E\left[e^{\rho_X\sigma_2\mathcal{J}}-1\right]=\frac{(1-p_X)\eta_2}{\eta_2+\rho_X\sigma_2}+\frac{p_X\eta_1}{\eta_1-\rho_X\sigma_2}-1.$$

In Equation (10), we disregard the effect of the factors h and ℓ in cases when a jump occurs, because they have negligible relative impact when ΔT is small. Also, we have not absorbed the correction terms (from Equation (2)) into the definition of ν_2, so as to show their explicit impact on the preceding equations.

One important note is that when we generate the tree on a logarithmic scale, the increment size for the discretisation is set by the value $\log h = -\log \ell = \sigma_2\sqrt{\Delta T\left(1-\rho_X^2\right)}$. If ρ_X approaches 1, this quantity will tend to zero, making the computation numerically intractable. It means that the random fluctuations in project value are almost entirely determined by the jump process, which is independent of the stock price. Thus, we choose an arbitrary upper bound of $\rho_X = 0.9$ when performing our calculations.

The parameter δ, the "below-equilibrium rate-of-return shortfall", is defined in Grasselli (2011) as the difference between the value of μ_2 related to the capital asset pricing model (CAPM) equilibrium and the actual value of μ_2. It satisfies the equation:

$$\delta = \rho\frac{\mu_1 - r}{\sigma_1}\sigma_2 + r - \mu_2, \tag{11}$$

which we maintain even though σ_2 encompasses the volatility associated with the jump-diffusion component of the project-value process.

We permit the discrete random variable ΔX_d to take on the values:

$$x_1, x_2, \ldots, x_n,$$

with probabilities:

$$\pi_1, \pi_2, \ldots, \pi_n,$$

respectively. The increment size for the discretisation ΔX_d is set by the value $\log h$. That is, each of the x_i values ($i = 1$ to n) must be a multiple of $\log h$, so that the tree recombines. The procedure we use for selecting the x_i and π_i parameters is provided in the following section.

We calculate the discounted option *continuation value* D_c. That is, the value of the option to the investor at time t, if they do *not* choose to exercise it then, following the derivation in (Grasselli 2011, Equation (35)), is equal to:

$$\begin{aligned} &D_c(t,V) = \\ &\frac{q}{\gamma_{t_0}} \log\left(\frac{p_1+p_2}{(1-\lambda\Delta T)\left[p_1 U_t(D^+)+p_2 U_t(D^-)\right]+\lambda\Delta T(p_1+p_2)\sum_{i=1}^{n}\pi_i U_t(D_i^+)}\right) \\ &+\frac{1-q}{\gamma_{t_0}} \log\left(\frac{p_3+p_4}{(1-\lambda\Delta T)\left[p_3 U_t(D^+)+p_4 U_t(D^-)\right]+\lambda\Delta T(p_3+p_4)\sum_{i=1}^{n}\pi_i U_t(D_i^+)}\right). \end{aligned} \tag{12}$$

In this equation,

$$\begin{aligned} q &= (1-d)/(u-d), \\ D^+ &\equiv D(t+\Delta T, \log(V(t))+\log h), \\ D^- &\equiv D(t+\Delta T, \log(V(t))-\log h), \\ D_i^+ &\equiv D(t+\Delta T, \log(V(t))+x_i), \end{aligned}$$

where $D(\cdot,\cdot)$ represents the discounted value of the option.

Finally, we calculated the discounted option value D, at time t, project value $V(t)$. It is equal to the *maximum* of the continuation value and the *immediate exercise value*, D_e. That is,

$$D(t, \log V(t)) = \max\left(D_c, D_e\right), \tag{13}$$

where

$$D_e = V(t) - I(t). \tag{14}$$

The preceding equations permit backwards induction to be performed on the tree.

3.3. Discretisation of the Random Variables

We now consider the selection of the parameters x_i and π_i, that is, the probability distribution of the discretisation of ΔX_d. In order to achieve this, we utilise an approach explained in Luceño (1999). Given two integer parameters—M, N— the method provides a recursive algorithm for generating a discrete approximation to a given continuous distribution, with the following three properties. Firstly, the two distributions share the same low-order moments up to moment $2N-1$. Secondly, their distribution functions (CDFs) coincide at at least $M+1$ points. Thirdly, the discrete distribution takes on $M \cdot N$ different values, that is, $n = M \cdot N$. For computational efficiency, it is preferable to keep the product $M \cdot N$ as small as possible, without sacrificing the accuracy of the approximation.

In implementing the approach, we selected M bands containing equal probability weight. That is, the $M+1$ points where the two distributions coincided corresponded to their 0, $100/M$, $200/M, \ldots,$ 100-th percentiles. In fact, the approach guarantees that exactly $N = 2$ discrete values occur between any pair of these successive percentiles.

In selecting values for M, N, note that the choice $N = 2$ guarantees that the three moment parameters—mean, variance, skewness—necessary to define a double-exponential distribution are preserved in the discretised form. We believe that, given an upper restriction for n, there is greater utility in increasing the parameter M, rather than selecting a value of N greater than 2. The discrete CDF will converge uniformly to the continuous CDF through the increasing number of coincident points, at equally spaced probability weights.

Finally, given $N = 2$, we have chosen M by acknowledging the trade-off between computational speed and the accuracy of the approximation. There is another consideration: following implicitly from the allocation of two discrete points for each of M bands, the maximum value of $|x_i|$ selected by the

algorithm will increase as M does. For the simplest case $p_X = 1/2$, $\eta_1 = \eta_2 = \sigma_2\rho_X$, if $M = 3, 4, 5, 6, 7$, then $\max\{|x_i|\} = 3.8, 4.1, 4.3, 4.5, 4.7$, respectively. By choosing a smaller value of M, we can reduce the size of the arrays we need to store in order to perform the backwards induction step of the process. This consideration is of greater significance when we have skewed distributions, with long tails in one direction. For example, if $p_X = 1/3$, $\eta_1 = \sigma_2\rho_X/\sqrt{2}$, $\eta_2 = \sqrt{2}\sigma_2\rho_X$, and $M = 3, 4, 5, 6, 7$, then $\max\{|x_i|\} = 4.8, 5.2, 5.6, 5.8, 6.0$, respectively.

Comparison between the continuous and discrete-approximation density functions, for these two cases ($p_X = 1/2, 1/3$), for $M = 3, 5$, are illustrated in Figure 1. In Figure 1a,b, two discrete values occur below the 33.3$^{\text{rd}}$ percentile and above the 66.7$^{\text{th}}$ percentile of the respective continuous distributions. For Figure 1c,d, the percentiles are the 20$^{\text{th}}$, 80$^{\text{th}}$ respectively. Thus, the most extreme values for the $M = 5$ case are more extreme than those for the $M = 3$ case (consistent with the earlier statements about $\max\{|x_i|\}$), but they have lower weight.

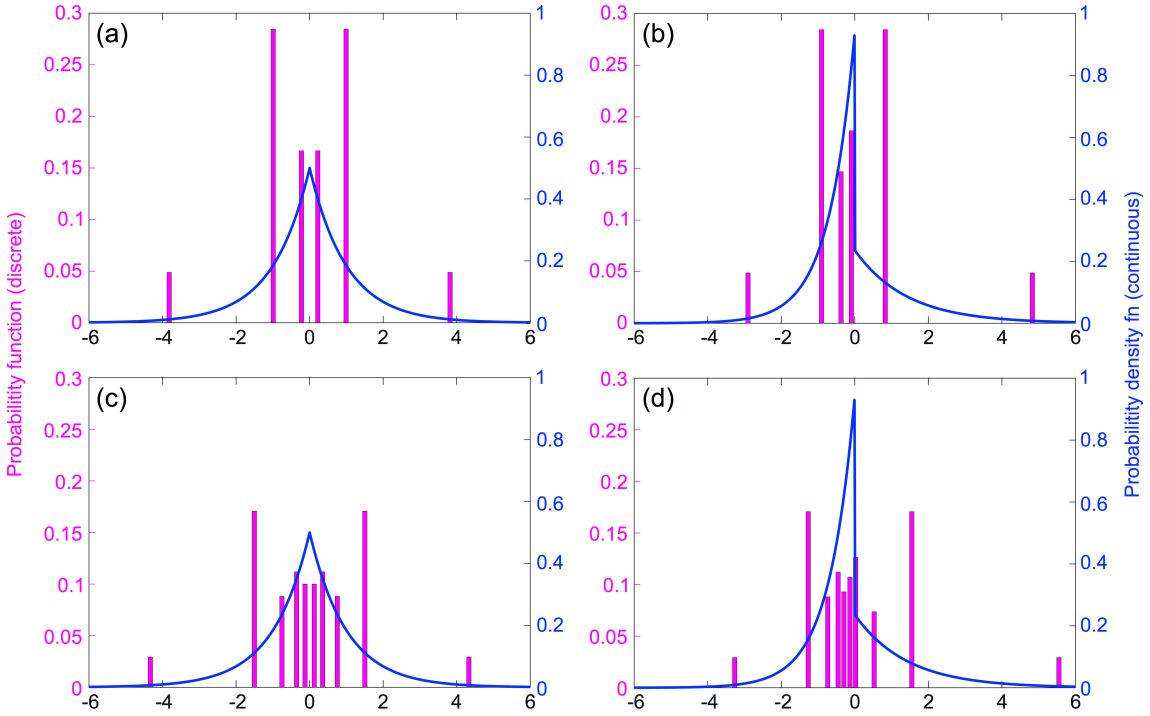

Figure 1. Comparison between the double-exponential density function and its discrete approximations for the cases: (**a**) $p_X = 1/2, M = 3, N = 2$; (**b**) $p_X = 1/3, M = 3, N = 2$; (**c**) $p_X = 1/2, M = 5, N = 2$; (**d**) $p_X = 1/3, M = 5, N = 2$.

Based on these considerations, we believe that $M = 5$ is a suitable compromise for providing both accuracy and computational efficiency. Some additional numerical analysis is provided in Section 5.3.1.

We also were required to round the $M \cdot N$ values for which the discrete distribution is defined to the nearest multiple of $\log h = \sigma_2\sqrt{\Delta T\left(1-\rho_X^2\right)}$. For small ΔT, the error introduced at this step will often be negligible, but we address the issue in more detail in Section 5.1.

4. Numerical Calculation

We proceed by listing the input parameters of the calculation. The fundamental parameters are T, μ_1, σ_1, σ_2, δ, ρ, ρ_X, α, i, r, λ, χ (or Sk_X), γ_0 and the numerical parameters are ΔT, M, N. The parameter μ_2 can be calculated using Equation (11).

Next, we must decide upon the sizes of the arrays (multinomial trees). The number of columns is set by T, ΔT, and is equal to $n_c = (T/\Delta T) + 1$. The set of times is $\{0, \Delta T, 2\Delta T, \ldots, T\}$. The number of rows is set by considering the maximum and minimum values of V for which the option price is

calculated, say $V_{\max}$, $V_{\min}$, respectively. We recall that V represents the value of the project at any given time, discounted at the risk-free rate to its present value at time $t = 0$.

The range of values of V, from $V_{\max}$ to $V_{\min}$, must be sufficiently broad so as not to affect the result of the simulation. Their influence on the calculation is through Equation (12), in which a weighted sum of the option values at time $t + \Delta T$ is required in the calculation of the *continuation* value of the option at time t. Suppose V^* is the *maximum* discounted exercise threshold over the interval $[0, T]$. That is, for any time $t \in [0, T]$, if the discounted project values exceeds V^*, we are guaranteed to exercise the option immediately, and we do not need to calculate the continuation value (or apply Equation (12)). Then $V_{\max}$ need be no greater than $V^* \exp(\max_i \{x_i\})$, according to the definition of D_i^+. Of course, V^* is not necessarily known precisely in advance of performing the calculation, however, a reasonable upper bound can be specified by adding a small margin to its value in known cases (for example, the $\rho_X = 0$ case).

The value of $V_{\min}$ need only be chosen so that the option value is near-zero, with reasonable tolerance, when the discounted project value lower than this value, at all times t. Such a value can be determined by trial and error, using the case $\rho_X = 0$, and then applied to more general cases as required.

Once $V_{\max}$, $V_{\min}$ are specified, the discrete values of V are evenly spaced on a logarithmic scale, with increment $\log h$. Thus, the number of rows is:

$$n_r = \left\lfloor \frac{\log(V_{\max}) - \log(V_{\min})}{\log h} \right\rfloor + 1, \tag{15}$$

where the "floor" notation indicates rounding down to the nearest integer.

We next generate the arrays. Firstly, we define the column vector $\mathbf{V}$ of values of V, as follows:

$$\mathbf{V} = \exp\left(\log h \left[\left\lfloor \frac{\log(V_{\min})}{\log h} \right\rfloor + (n_r - 1), \left\lfloor \frac{\log(V_{\min})}{\log h} \right\rfloor + (n_r - 2), \ldots, \left\lfloor \frac{\log(V_{\min})}{\log h} \right\rfloor \right]^T \right), \tag{16}$$

where the superscript T represents matrix transpose, and the exponentiation operator is applied to each element individually.

Next, we consider the matrix of option values, $\mathcal{D}$, which has dimensions $n_r \times n_c$. Each row corresponds to a different value of the project value; each column to a different time step.

The rightmost column, column n_c, corresponds to time T. At this time, the option has no continuation value, and its value is equal to its exercise value (both discounted to time $t = 0$), so that (Grasselli 2011, Equation (53)):

$$\mathcal{D}[\cdot, n_c] = (\mathbf{V} - \exp[(\alpha - r)T]\, \mathbf{I}_0)_+, \tag{17}$$

where $\mathbf{I}_0$ is an $n_r \times 1$ vector with all entries equal to $I(0)$, and the notation on the left-hand side represents the n_c-th column of $\mathcal{D}$.

Next, backward induction is applied to columns $j = n_c - 1, n_c - 2, \ldots, 2, 1$ in this order. To do so, Equation (12) is applied point by point to the values in the vector $\mathbf{V}$. For calculation efficiency, in calculating the entry $D_c(t(j), \log V(t))$, corresponding to column j of the array, we only need to be concerned with values of $V(t)$ that are below the exercise threshold for the column, noting that this is not known precisely in advance for each value of j. For higher values of $V(t)$, the discounted option value is equal to the immediate exercise value.

However, the calculation for $D_c(t(j), \log V(t))$ may make reference to out-of-bound entries of the vector $\mathcal{D}[\cdot, j + 1]$, if V is particularly low (near $V_{\min}$). Note that appropriate selection of $V_{\max}$ should avoid this problem in the high-V case. This is due to the limited range of project values for which the option continuation value is calculated, as explained in the previous paragraph. In the low

case, we may substitute zero for out-of-bound values, which should be appropriate according to the selection of $V_{\min}$.

The discounted immediate exercise value of the option at the j-th column is given by the vector:

$$\mathbf{D}_e = \mathbf{V} - \exp\left[(\alpha - r)(j-1)\Delta T\right]\mathbf{I}_0, \tag{18}$$

and is permitted to be negative.

The discounted option value vector $\mathbf{D} = \max(\mathbf{D}_c, \mathbf{D}_e)$, where the maximum operation is performed element by element. The exercise threshold is the $V(t)$ value for which $D_c = D_e$. This threshold may be calculated using linear interpolation, given the two vectors. Then $\mathcal{D}[\cdot, j] = \mathbf{D}$.

The backward-induction operations can be performed on a column-by-column basis (instead of an element by element basis), using a convolution operation to implement Equation (12) step, applied to the denominators of the arguments of the log functions. This is useful from the perspective of calculation efficiency, especially given the few values for x_i required in our discretisation approach.

Finally, for display purposes, we have chosen to re-scale the array so that each row corresponds to a constant undiscounted project value, rather than a constant discounted value. (The discounting step is a mathematical convenience introduced at the start of the calculation, to the somewhat arbitrary choice of time $t = 0$.) Noting that the (vertical) project-value scale is expressed in logarithmic units, this is achieved by translating each column in the array by the appropriate amount to reverse the effect of discounting. Interpolation is used to deal with translations of fractional units of $\log h$. The figures presented in the next section are adjusted in this way. Similarly, the option values displayed in the figures are in undiscounted values, calculated by multiplying the discounted option values D, by $\exp(rt)$.

The process allows us to calculate option exercise threshold at each point in time, the option value for every combination of project value and time. The option value can be split into *time value* and *money value*, and it is convenient to display the former in the figures. The value of the option when "at the money" is also plot against time. It may be calculated by interpolation from the derived array $\mathcal{D}$, and considered along with the exercise threshold (at time $t = 0$) as a means of comparing the results when the input parameters are modified.

5. Simulation Results

We performed numerical calculations using Matlab 2016a on a PC with an Intel (R) Core (TM) i7-6700HQ CPU @ 2.60 GHz, and 16 GB RAM, on Windows 10 (64-bit).

We utilised the following parameters, unless stated otherwise, following Grasselli (2011). Fundamental parameters: $\mu_1 = 0.115$; $\sigma_1 = 0.25$; $\sigma_2 = 0.2$; $\delta = 0.04$; $\rho = 0.5$; $\alpha = 0$; $r = 0.04$; $\gamma_0 = 2$. The selected numerical parameter ΔT was usually chosen to be 0.0005, with exceptions noted in the text where applicable.

5.1. Time-Dependent Utility Function

In the first instance, we set $\rho_X = 0$, so that there is no jump-diffusion component to the project price movements. Figure 2 shows the difference between the cases where $\alpha = i$ and $r = i$. The vertical axis represents the undiscounted project value, $\tilde{V}$, plotted on a logarithmic scale. The horizontal axis is shown on a reverse scale indicating time to expiry. Thus, actual time t runs from left to right, beginning at $t = 0$. This is explicitly indicated in Figure 2d.

The colour scale in the two-dimensional array represents the undiscounted *time value* of the option, which is greatest when the option is approximately at the money. For each panel of the figure, the blue dotted line indicates time/project-value combinations for which the option is at the money. Since the inflation rate $\alpha = 0$, this is a horizontal line at project value 1. The green dotted line, drawn parallel to the blue line, represents (at time $t = 0$) the exercise threshold in the limit $T \to \infty$. Finally, the red

dotted line represents the exercise threshold throughout the lifetime of the option, above which the time value of the option is zero.

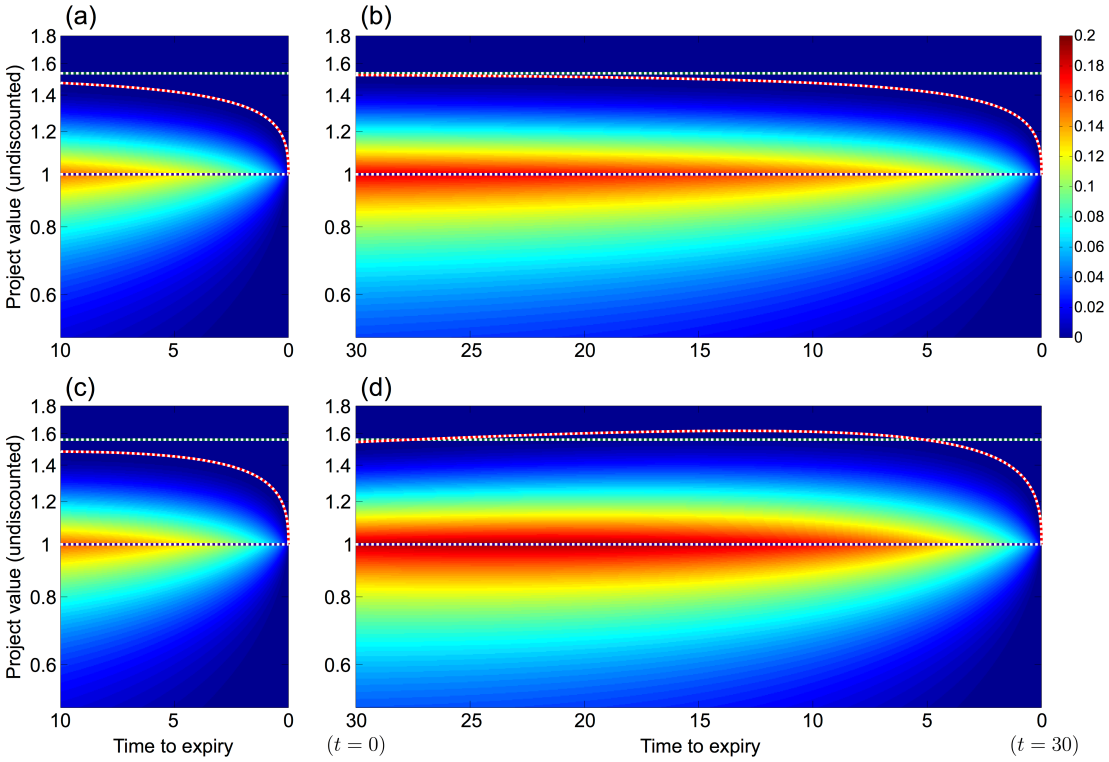

Figure 2. (**a**) Case $T = 10$, $\alpha = i$. Colour scale represents the undiscounted time value of the real option. The vertical axis (undiscounted project value) is plotted with a logarithmic scale. Time is plotted on the horizontal axis. Blue line: at the money; Red line: exercise threshold; Green line: Infinite-maturity exercise threshold; (**b**) Case $T = 30$, $\alpha = i$; (**c**) Case $T = 10$, $r = i$; (**d**) Case $T = 30$, $r = i$. Exercise threshold at $t = 0$: (**a**) 1.4731; (**b**) 1.5226; (**c**) 1.4816; (**d**) 1.5425. Option value at the money ($t = 0$): (**a**) 0.1531; (**b**) 0.1797; (**c**) 0.1564; (**d**) 0.1881. Calculation time (backwards induction step): (**a**) 1.37 s; (**b**) 5.37 s; (**c**) 1.38 s; (**d**) 5.31 s.

In the top row, for which $\alpha = i$, Figure 2a, for which $T = 10$, is identical to the rightmost region of the Figure 2b ($T = 30$). This is because, in the absence of inflation (in either the option contract or the option-holder's preferences), the situation faced by the option-holder 10 time units prior to expiry does not depend on the value of T. The red curves are strictly increasing as time to expiry increases, that is, looking from right to left, representing the corresponding increasing benefit of holding the option.

In the case $r = i$ (lower row of Figure 2), once again, the red curve lies strictly below the green line at time $t = 0$, representing the greater value of an option with a longer time to expiry. However, in this case, specifically in Figure 2d, the decision threshold (red curve) is not necessarily decreasing over the lifetime of the option. This surprising effect is due to the fact that the option-contract-specific inflation rate, α, is lower than the investor's implied inflation rate, i. Thus, for large values of t, the option-holder is less risk-averse with respect to monetary values equal to the strike price, so is more likely to delay exercising the option. Just as the exercise threshold increases over the life of the option, similarly, the option value at the money increases prior to decreasing to zero at expiry.

To avoid this counterintuitive result, we believe it is more sensible and realistic to adopt the approach that $\alpha = i$, so that both at-the-money option value and the exercise threshold are decreasing functions of time. If a known alternative effective inflation rate can be assigned to the investor, this value should be used instead.

The calculation times (in seconds) for the backwards induction step (i.e., generating the two-dimensional arrays) are provided in the figure caption. They are the averaged results of three trials in each case. These times are clearly dependent on the sizes of the arrays. The $T = 30$ values are almost four times as large as the $T = 10$ values, due to the additional computational resources required to progressively update the larger arrays.

5.2. Inflation Effects

Given $\alpha = i$, we consider the effect as this parameter is varied. Figure 3 presents plots in the manner of Figure 2, for the cases (a) $\alpha = i = 0.01$, (b) $\alpha = i = 0$, and (c) $\alpha = i = -0.01$. The parameter $T = 20$, and all other parameters are as given at the beginning of this section. In each case, the (red) exercise threshold curve approaches the (blue) at-the-money line as time t increases, a consequence of the two inflation parameters being equal.

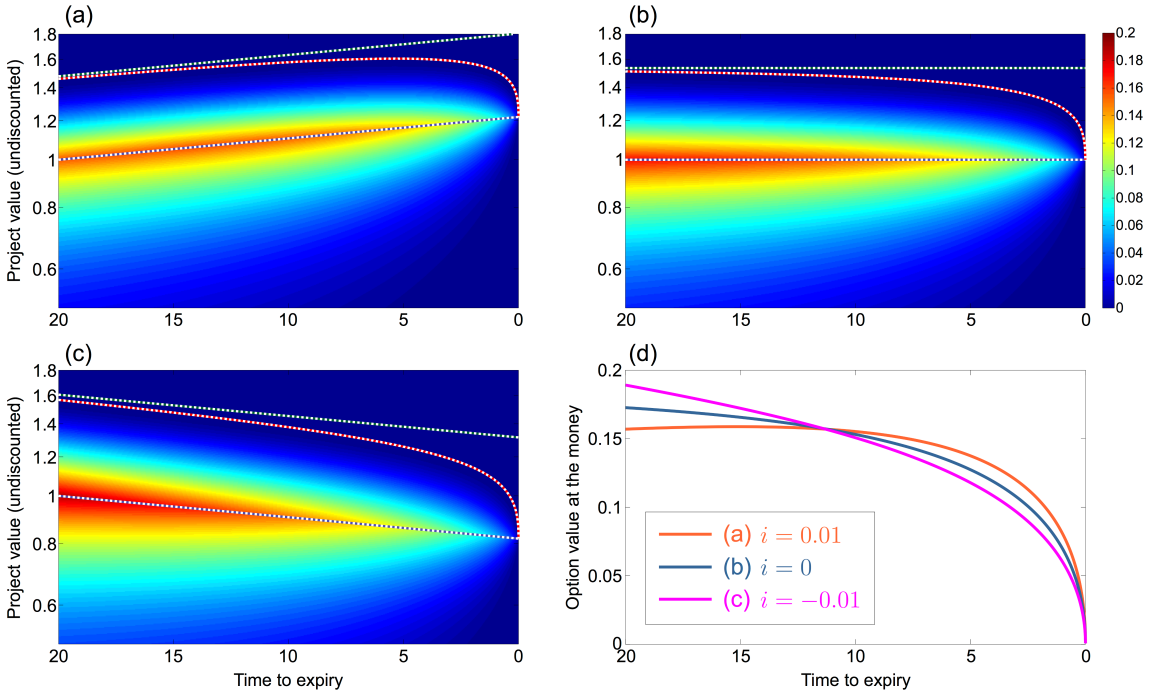

Figure 3. (**a**) Case $T = 20$, $\alpha = i = 0.01$. Colour scale represents the undiscounted time value of the real option. The vertical axis (undiscounted project value) is plotted with a logarithmic scale, and the horizontal axis represents time. Blue line: at the money; Red line: exercise threshold; Green line: Infinite-maturity exercise threshold. (**b**) Case $T = 20$, $\alpha = i = 0$. (**c**) Case $T = 20$, $\alpha = i = -0.01$.; (**d**) Plot of undiscounted option value at the money, versus time to expiry, for the three cases represented in (**a**–**c**). Exercise threshold at $t = 0$: (**a**) 1.4593; (**b**) 1.5102; (**c**) 1.5652. Option value at the money ($t = 0$): (**a**) 0.1570; (**b**) 0.1727; (**c**) 0.1892. Calculation times (backwards induction step): (**a**) 3.26 s; (**b**) 3.19 s; (**c**) 3.61 s.

The at-the-money option value at time $t = 0$ is greatest when $\alpha = i = -0.01$, and least when $\alpha = i = 0.01$. This is because the option is more likely to be "in the money" at any point in the future, if inflation (as specified in the option contract) is lower (or negative). Similarly, the exercise threshold increases for decreasing α, i.

However, the at-the-money option value decreases much more sharply with time t as inflation decreases, as shown in Figure 3d, so that eventually (towards the right of the panel), the order of the three curves is reversed. This effect can be ascribed to the fact that the actual monetary values on the at-the-money line increase/decrease according to inflation/deflation, which will contribute a scaling

effect to the option value. In fact, the curve for the positive-inflation case is actually increasing with t for a subset of its domain (low values of t).

The reported calculation times, provided in Figure 3 caption, are consistent with the values provided in Figure 2, given T. The slight differences between them are due to the different maximum and minimum values of V (and hence the sizes of the arrays) for the different cases (and random variation).

5.3. Incorporation of Jump Diffusion into the Project Value

We now restrict ourselves to the case $\alpha = i = 0$ in order to compare the results as the jump-diffusion parameters are varied. This permits us to avoid the issues described in the previous sections, including the scaling issue that occurred when the project value at the money varied over the lifetime of the option. The results are presented in successive figures. As noted in Section 3.3, we used the values $M = 5$, $N = 2$ to perform the calculations.

5.3.1. Effect of Varying the Parameter ρ_X

In Figure 4, a jump-diffusion model is presented with the parameters $\lambda = 0.1, \chi = 1$. The latter parameter choice means that upwards and downwards jumps are equally likely. Results are displayed for different values of ρ_X. [The ratio $\rho_X^2/(1-\rho^2)$ is the relative contribution by variance of the jump-diffusion component to the project-value fluctuations that are independent of the stock index movements.]

Despite the fact that we have controlled for the drift and volatility of the project-value process, the net effect of introducing jump diffusion into the model is to reduce the option value and exercise threshold, as indicated in the figure. The risk-averse investor responds negatively to the possibility of extreme changes in project value, valuing the option less and being more likely to exercise it early, if the other parameters are held stable.

Figure 4e shows that the relative option values for different ρ_X cases remain stable over the option's lifetime, and Figure 4f presents a comparison between the continuous double-exponential probability density function and its discrete approximation. Up to rounding of the x_i values, the discrete and continuous cumulative distribution functions match at the quintiles of the latter, and the first three moments agree. Due to the symmetry about the origin for the case $\chi = 1$, the distributions also have equal medians.

The calculation times provided in Figure 4 are also provided as multiples of the $\rho_X = 0$ case, so that the computational cost of incorporating jump diffusion into the model is quantified. This cost comes about from two sources: firstly, the incorporation of the n-term sums into Equation (12), recalling that $n = M \cdot N$; and secondly, the increased sizes of the arrays required when ρ_X is large (to accommodate larger jumps). The effect of the first source in isolation can be approximated by considering the low-$\rho_X = 0.5$ case. The additional computational burden is quite modest (relative computation time 1.3×). The value increases to 1.9× for the $\rho_X = 0.8$ case, for which the jumps are the dominant source of stochastic variation in the project value. This may be accounted for by the second source identified above; it reflects the concomitant increase in the array size.

We also use this scenario to compare the effects on the results and calculation time when the computation parameters M and N are modified. Firstly, we consider three cases for the pair (M, N), as presented in Table 1. Our choice of selected parameters provides similar exercise thresholds and option values at the money to those of the higher values $(M, N) = (6, 3)$. However, the calculation times are only modestly greater than those of the $(M, N) = (3, 2)$ case, to within $\approx 0.1\times$ the respective $\rho_X = 0$ calculation times. These observations suggest that our choice is a reasonable compromise between accuracy and computation speed.

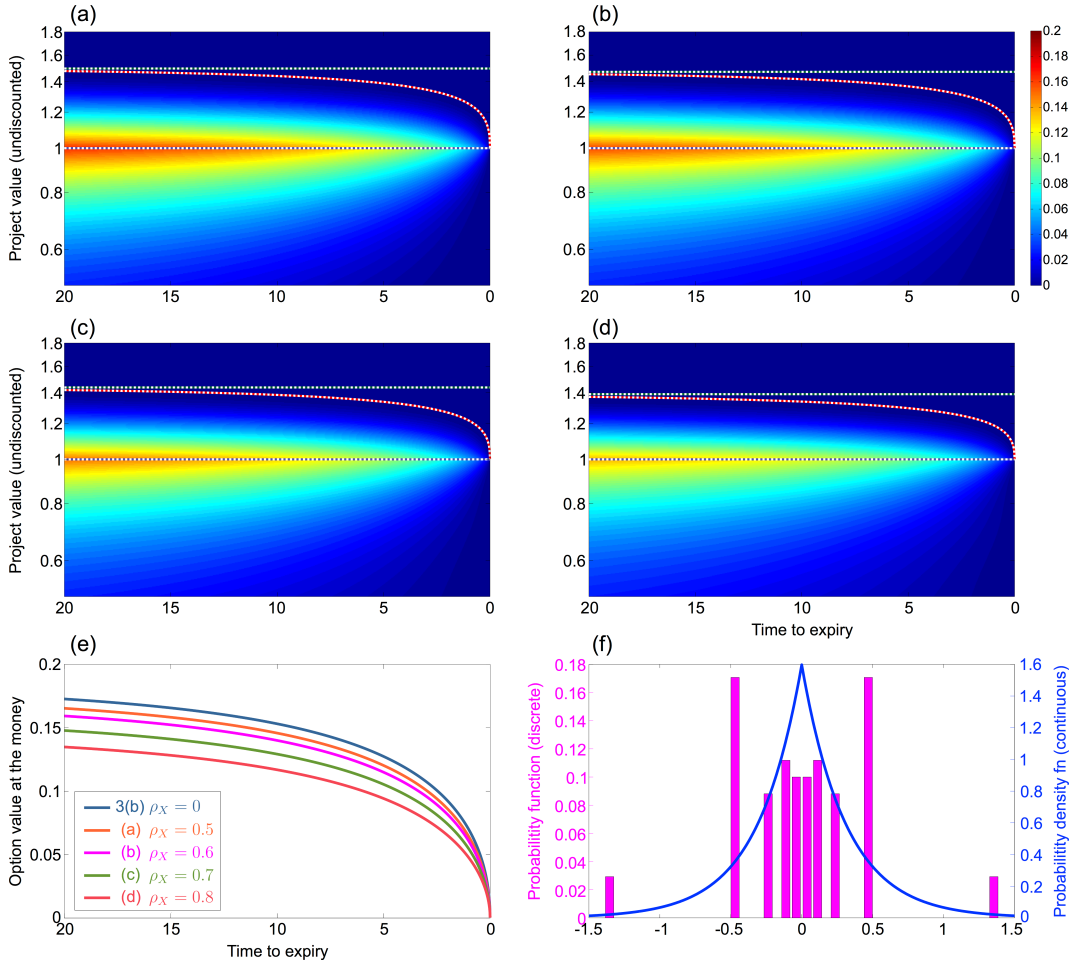

Figure 4. Process as in Figure 3b, but incorporating jump diffusion with parameters $\lambda = 0.1, \chi = 1$. The parameter ρ_X is, sequentially: (**a**) 0.5; (**b**) 0.6; (**c**) 0.7; (**d**) 0.8. Sub-figure (**e**) Plot of undiscounted option value at the money, versus time to expiry, for the four cases represented in (**a**–**d**). Sub-figure (**f**) Continuous and discrete (incorporating rounding of the x_i values) approximations of the random variable $\sigma_2 \rho_X \Delta X$, for the case $\rho_X = 0.6$. Exercise threshold at $t = 0$: (**a**) 1.4736; (**b**) 1.4483; (**c**) 1.4105; (**d**) 1.3563. Option value at the money ($t = 0$): (**a**) 0.1653; (**b**) 0.1588 (**c**) 0.1490; (**d**) 0.1348. Calculation times (backwards induction step): (**a**) 4.07 s (1.3×); (**b**) 4.48 s (1.4×) ; (**c**) 4.98 s (1.6×); (**d**) 6.14 s (1.9×), where the figures in parentheses represent a multiple of the $\rho_X = 0$ case of Figure 3b.

Table 1. Exercise thresholds (ET), option values at the money (OVATM), calculation times (backwards induction step) (CT), for multiple simulations of the process. The centre columns correspond to Figure 3b ($\rho_X = 0$), and Figure 4a–d ($\rho_X = 0.5, 0.6, 0.7, 0.8$, respectively). The other columns were generated through changing only the values of M, N as indicated. Figures in parentheses represent calculation times as a multiple of the $\rho_X = 0$ case.

ρ_X	$M = 6, N = 3$			$M = 5, N = 2$			$M = 3, N = 2$		
	ET	**OVATM**	**CT (s)**	**ET**	**OVATM**	**CT (s)**	**ET**	**OVATM**	**CT (s)**
0	1.510	0.173	3.19	1.510	0.173	3.19	1.510	0.173	3.19
0.5	1.474	0.166	4.53 (1.4×)	1.474	0.165	4.07 (1.3×)	1.473	0.165	3.98 (1.2×)
0.6	1.449	0.159	5.21 (1.6×)	1.448	0.159	4.48 (1.4×)	1.447	0.158	4.46 (1.4×)
0.7	1.411	0.150	5.94 (1.9×)	1.411	0.149	4.98 (1.6×)	1.409	0.148	4.83 (1.5×)
0.8	1.357	0.136	7.34 (2.3×)	1.356	0.135	6.1 (1.9×)	1.354	0.133	5.88 (1.8×)

5.3.2. Effect of Varying Jump Rate λ

Figure 5 illustrates the effect of modifying the parameter λ, when other parameters are held constant. Note that if the jump rate is increased, but the drift and volatility remain constant, then the jump size must necessarily decrease. Also, according to the central limit theorem, as λ increases indefinitely, the jump process should tend towards the Brownian motion process W_t^2. That is, the model should approach the case for which $\rho_X = 0$. This observation is borne out in Figure 5f. Beginning at the case $\lambda = 0.1$, from Figure 4d, the option value curve rises steadily as λ is increased to (a) 0.2, (b) 0.3, (c) 0.5, (d) 1, then (e) 2, ultimately approximating the case $\rho_X = 0$ from Figure 3b. Again, the relative option value remains consistent over the entire time to expiry.

The differences in calculation times listed reflect the second source of costs mentioned in Section 5.3.1, that is, different array sizes. The calculation times also reflect the first source (additional calculations per induction step), even for high values of λ, when the result is similar to the case $\rho_X = 0$. Given these considerations, the times listed are consistent with those of Section 5.3.1.

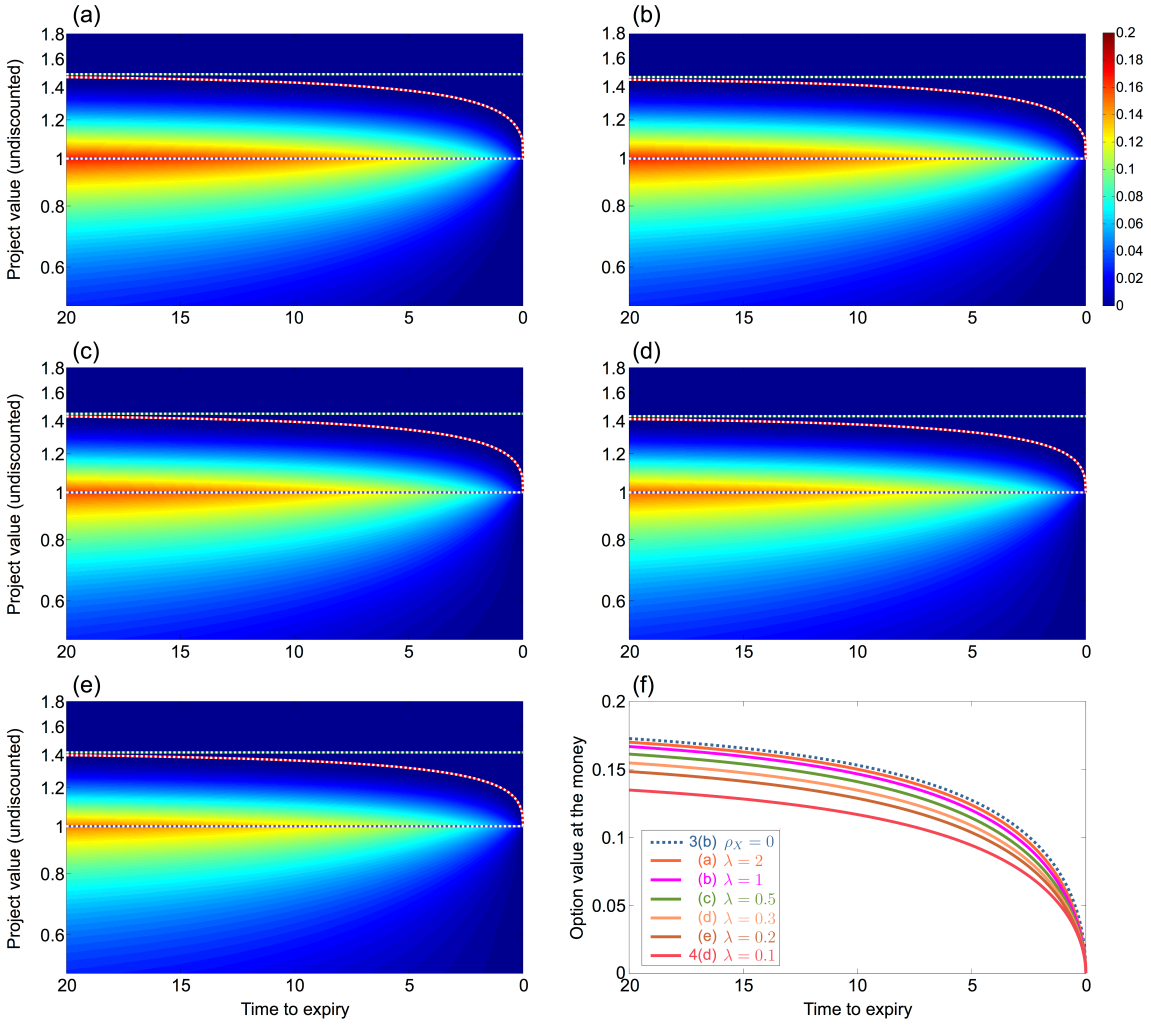

Figure 5. As in Figure 4d, but with jump rates λ equal to: (**a**) 2; (**b**) 1; (**c**) 0.5; (**d**) 0.3; (**e**) 0.2. (**f**) Plot of undiscounted option valuen at the money, versus time to expiry, for the five cases represented in (**a**–**e**). Exercise threshold at $t = 0$: (**a**) 1.4664; (**b**) 1.4481; (**c**) 1.4272; (**d**) 1.4075; (**e**) 1.3902. Option value at the money ($t = 0$): (**a**) 0.1700; (**b**) 0.1668 (**c**) 0.1613; (**d**) 0.1548; (**e**) 0.1484. Calculation times (backwards induction step): (**a**) 4.37 s (1.4×); (**b**) 4.52 s (1.4×) ; (**c**) 4.84 s (1.5×); (**d**) 5.06 s (1.6×); (**e**) 5.46 s (1.7×), where the figures in parentheses represent a multiple of the $\rho_X = 0$ case of Figure 3b.

5.3.3. Effect of Varying Skewness Sk_X

In Figure 6, starting with the parameters used to generate Figure 4b, we investigate the effect of modifying the skewness parameter Sk_X from the value 0 which has been utilised thus far.

We used the values $\mathrm{Sk}_X = -3$, 0 and 3, corresponding to $\chi = 0.268, 1$ and 3.73 respectively. In Figure 6c, we see that the largest at-the-money option value occurs when $\mathrm{Sk}_X = -3$ (that is, 0.1614), with value falling to 0.1588 for zero skewness, and much further to 0.1359 for skewness +3. The asymmetry of this effect (about zero skewness) is due to the different characteristics of the upside and downside risks associated with jumps in the positive- and negative-skewness cases, noting that the value of an option lies in its ability to eliminate downside risk. Specifically, in the positive-skewness case, most jumps are downwards and small in magnitude, with a few being upwards and large in magnitude. However, these directions are reversed in the negative-skewness case. (We emphasise again that all effects must be understood in the context that drift and volatility are held constant in the project-value process.) In Section 5.3.4, we will see that the effect of increasing λ rapidly mitigates the limited-downside-risk issue associated with the positive-skewness case.

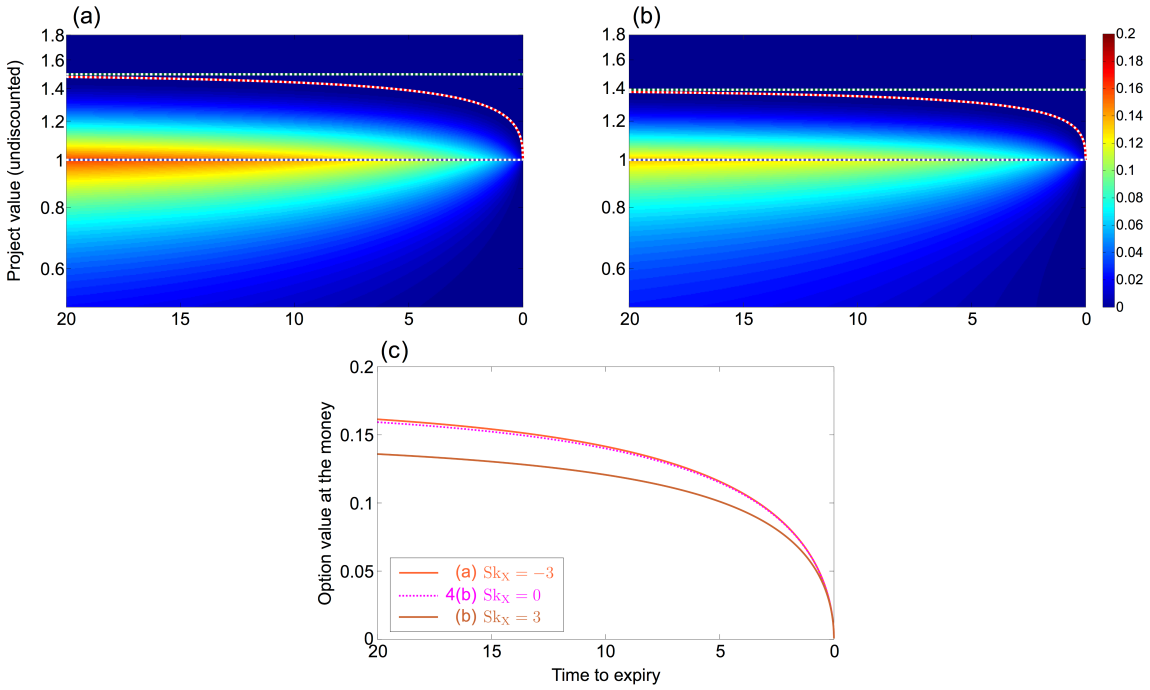

Figure 6. As in Figure 4b, but with skewness Sk_X equal to: (**a**) -3; (**b**) 3; (**c**) Plot of undiscounted option value at the money, versus time to expiry, for the three cases in $\mathrm{Sk}_X = -3, 0, 3$. Exercise threshold at $t = 0$: (**a**) 1.4767; (**b**) 1.3762. Option value at the money ($t = 0$): (**a**) 0.1614; (**b**) 0.1359. Calculation times (backwards induction step): (**a**) 4.12 s; (**b**) 5.04 s.

The optimal exercise threshold exhibits a similar dependence on skewness, being also asymmetric about the origin. The listed calculation times, comparable with the 4.48 s from Figure 4b, tend to increase for greater values of skewness. This is due to different sizes of the required arrays (the second "source" of computational cost from Section 5.3.1), due to the fact that a lower value of $V_{\min}$ must be selected if larger positive jumps are possible.

5.3.4. Further Investigation of ρ_X, λ, Sk_X

In Figures 7 and 8, we plot exercise threshold and option value at time $t = 0$ for a range of input parameters. For Figure 7, we plot the variation of these quantities with jump rate λ, for three

different values of skewness Sk_X. We selected $\rho_X = 0.6$, $T = 10$, with all other parameters being equal to their values stated earlier.

The three coloured curves in the figure represent the different skewness levels. Their orderings for low values of λ are consistent with the discussion of Figure 6. Moreover, as observed with respect to Figure 5, the curves should converge to the black dotted line (representing the case $\rho_X = 0$) when λ increases indefinitely. This is apparent in the plots, although there are still discernible discrepancies between the curves even when $\lambda = 12$, representing 120 expected jumps over the option lifetime.

Another significant observation in the option-value plot is that when λ increases, the positive-skewness curve exceeds the zero- and negative-skewness curves and even apparently overshoots the large-λ limit. (This observation does not hold for the exercise-threshold plot.) This can be explained in terms of the rapid mitigation of the issue implied in the discussion of Figure 6, that the project-value jumps had limited downside risk, diminishing the option value. When a large number of jumps occur, then the potential cumulative effect of multiple downward jumps does constitute more significant downside risk when considering the project value. So the option will gain value as a result.

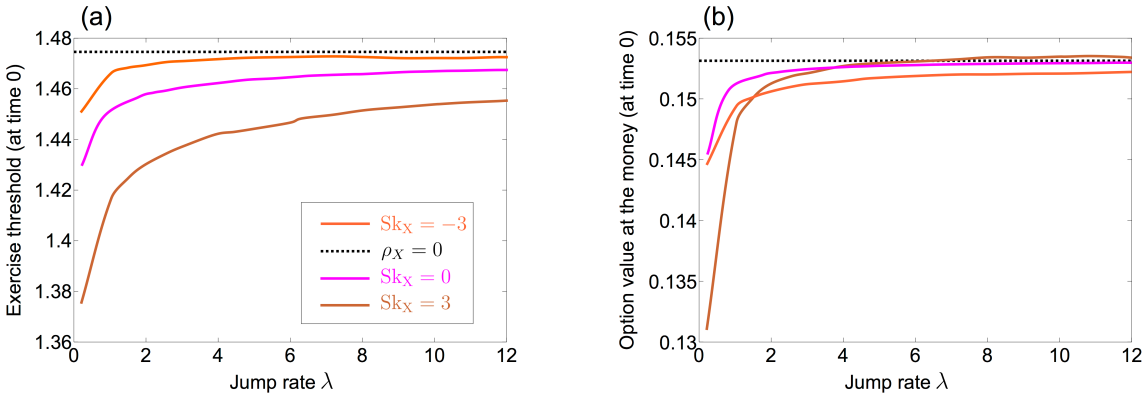

Figure 7. Plots of exercise threshold (**a**) and option value (**b**) at time $t = 0$, vs. jump rate λ, for different values of skewness $(-3, 0, 3)$. Other parameters are given in the text. In particular, $\rho_X = 0.6$. The comparison level when $\rho_X = 0$ is indicated using a black dotted line.

The small-scale fluctuations in the plotted curves are due to calculation noise, in particular, the rounding error associated with forcing the values of x_i to be multiples of $\log h$. This effect has been mitigated by selecting $\Delta T = 0.00005$ for Figure 7, as opposed to the value $\Delta T = 0.0005$ used earlier. Also, the effect is only significant for large values of λ (for which the jump size, compared to $\log h$, is relatively small). The curves have been smoothed, partly through the judicious choices of the discrete jump rates λ for which they were calculated. For these reasons, particularly in Figure 7b, the plotted values have limited reliability for large values of λ. Finally, we note that the error is least when $\mathrm{Sk}_X = 0$, since in this case the first and third moments of the discrete distribution are guaranteed to be matched to those of the continuous distribution it is approximating (i.e., to zero).

For Figure 8, we fix the value of λ at 0.1 (and set ΔT to 0.00025), and now plot the variation in exercise threshold and option value with skewness Sk_X. The trend observed in Figure 4 is apparent: the plotted quantities decline with increasing ρ_X, and this is preserved over all values of skewness. Additionally, as discussed in relation to Figure 6, the plotted quantities are asymmetric with respect to the sign (positive or negative) of the skewness. In particular, the low option value for large positive values of skewness is due to the fact that jumps are rare. (The expected number of jumps over the option's lifetime is 1.) The optimum level of skewness, in terms of maximising option value, is negative, and becomes more so as ρ_X is increased.

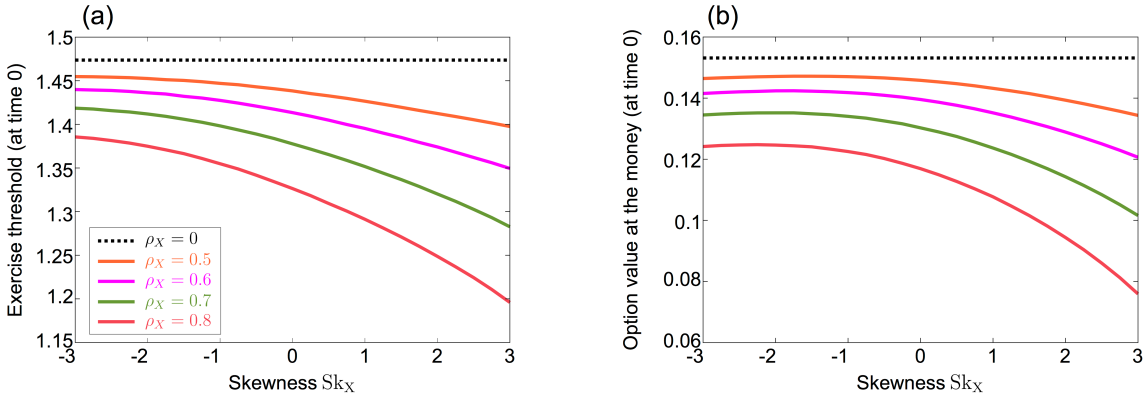

Figure 8. Plots of exercise threshold (**a**) and option value (**b**) at time $t = 0$, vs. skewness Sk_X, for different values of ρ_X (0, 0.5, 0.6, 0.7, 0.8). Other parameters are given in the text. In particular, $\lambda = 0.1$.

6. Conclusions

In this manuscript, we have incorporated two extensions to the real-options approach of Grasselli (2011). In doing so, we have maintained its key characteristics: the finite time horizon; the partial correlation between the project value and tradable instruments; and the utilisation of the investor's utility function.

In addition, we have incorporated the ability to model the investor's implied inflation rate, which determines the time dependence of their utility function. This permits us to perform a more realistic model of the investor behaviour over time, specifically, that an investor's risk preferences will tend to vary with inflation rather than the rate of interest.

Also, we have incorporated a jump-diffusion component into the value of the underlying project for which the option is written. In the most general case, the dominant effects of such a jump component would be the additional drift and volatility it imparted to the project value. Accordingly, we have limited the number of free parameters when defining our jump process, so as to control for these effects. The correction terms in Equation (2) also assist in this aim. As a result, we are able to examine the impact of the particular form of the double-exponential jump distribution, and the dependence of the option value and investor behaviour on the skewness of the jump process.

In the results we presented, the incorporation of a jump-diffusion component into the option price model tended to reduce both the exercise threshold and the option value. An apparent exception to this rule was shown in Figure 7b, in which it was possible for the plotted option value under the jump process to exceed that in its absence. However, this applied only for extremely high jump rates, and was subject to numerical error.

We have been able to utilise a parsimonious approach for approximating the continuous double-exponential distribution using a discrete distribution, taking only a limited number of values over the binomial tree whose increments are determined by the non-jump components of the process. As such, the additional computational burden of incorporating the jump-diffusion extension is small. Indeed, we found calculation times were generally less than twice those required in the absence of jump diffusion, except for cases of extreme values of the parameters.

Author Contributions: The authors contributed equally to this work.

Funding: This research was funded by Faculty Research Grant of University of Melbourne.

Acknowledgments: The authors are grateful to the anonymous reviewers whose valuable comments and suggestions have helped improve the paper and clarify the presentation.

Conflicts of Interest: The authors declare no conflict of interest. The founding sponsors had no role in the design of the study; in the collection, analyses, or interpretation of data; in the writing of the manuscript, and in the decision to publish the results.

References

Ainslie, George. 1992. *Picoeconomics*. Cambridge: Cambridge University Press.

Alonso-Bonis, Susana, Valentin Azofra-Palenzuela, and Gabriel De La Fuente-Herrero. 2009. Real option value and random jumps: Application of a simulation model. *Applied Economics* 41: 2977–89. [CrossRef]

Cai, Ning, and Steven G. Kou. 2011. Option pricing under a mixed-exponential jump diffusion model. *Management Science* 57: 2067–81. [CrossRef]

Chen, Shumin, Zhongfei Li, and Yan Zeng. 2014. Optimal dividend strategies with time-inconsistent preferences. *Journal of Economic Dynamics and Control* 46: 150–72. [CrossRef]

Cox, John C., Stephen A. Ross, and Mark Rubinstein. 1979. Option pricing: A simplified approach. *Journal of Financial Economics* 7: 229–63. [CrossRef]

Dixit, Avinash K., and Robert S. Pindyck. 1994. *Investment Under Uncertainty*. Princeton: Princeton University Press.

Grasselli, Matheus. 2011. Getting real with real options: A utility-based approach for finite-time investment in incomplete markets. *Journal of Business Finance and Accounting* 38: 740–64. [CrossRef]

Grenadier, Steven R., and Neng Wang. 2007. Investment under uncertainty and time-inconsistent preferences. *Journal of Financial Economics* 84: 2–39. [CrossRef]

Henderson, Vicky. 2007. Valuing the option to invest in an incomplete market. *Mathematics and Financial Economics* 1: 103–28. [CrossRef]

Hugonnier, Julien, and Erwan Morellec. 2007. Corporate control and real investment in incomplete markets. *Journal of Economic Dynamics and Control* 31: 1781–800. [CrossRef]

Kou, Steven G., and Hui Wang. 2004. Option pricing under a double exponential jump diffusion model. *Management Science* 50: 1178–92. [CrossRef]

Loewenstein, George, and Drazen Prelec. 1992. Anomalies in intertemporal choice: Evidence and an interpretation. *The Quarterly Journal of Economics* 57: 573–98. [CrossRef]

Luceño, Alberto. 1999. Discrete approximations to continuous univariate distributions—An alternative to simulation. *Journal of the Royal Statistical Society B* 61: 345–52. [CrossRef]

Merton, Robert C. 1976. Option pricing when underlying stock returns are discontinuous. *Journal of Financial Economics* 3: 125–44. [CrossRef]

Pham, Huyen. 1997. Optimal stopping, free boundary, and American option in a jump-diffusion model. *Applied Mathematics and Optimization* 35: 145–64. [CrossRef]

Song, Qingshuo, George Yin, and Zhimin Zhang. 2006. Numerical method for controlled regime-switching diffusions and regime-switching jump diffusions. *Automatica* 42: 1147–57. [CrossRef]

Thaler, Richard. 1981. Some empirical evidence on dynamic inconsistency. *Economics Letters* 8: 201–7. [CrossRef]

Yong, Jiongmin. 2012. Time-inconsistent optimal control problems and the equilibrium HJB equation. *Mathematical Control and Related Fields* 2: 271–329. [CrossRef]

Zhao, Qian, Jiaqin Wei, and Rongming Wang. 2014. On the dividend strategies with non-exponential discounting. *Insurance: Mathematics and Economics* 58: 1–13. [CrossRef]